Dual Stretch Responses of mHCN2 Pacemaker Channels: Accelerated Activation, Accelerated Deactivation

Wei Lin, Ulrike Laitko, Peter F. Juranka, and Catherine E. Morris
Neuroscience, Ottawa Health Research Institute, Ottawa Hospital, Ottawa, Ontario, Canada K1Y 4E9

ABSTRACT Mechanoelectric feedback in heart and smooth muscle is thought to depend on diverse channels that afford myocytes a mechanosensitive cation conductance. Voltage-gated channels (e.g., Kv1) are stretch sensitive, but the only voltage-gated channels that are cation permeant, the pacemaker or HCN (hyperpolarization-activated cyclic nucleotide-gated) channels, have not been tested. To assess if HCN channels could contribute to a mechanosensitive cation conductance, we recorded I_{HCN} in cell-attached oocyte patches before, during, and after stretch for a range of voltage protocols. I_{mHCN2} has voltage-dependent and instantaneous components; only the former was stretch sensitive. Stretch reversibly accelerated hyperpolarization-induced I_{mHCN2} activation (likewise for I_{spHCN}) and depolarization-induced deactivation. HCN channels (like Kv1 channels) undergo mode-switch transitions that render their activation midpoints voltage history dependent. The result, as seen from sawtooth clamp, is a pronounced hysteresis. During sawtooth clamp, stretch increased current magnitudes and altered the hysteresis pattern consistent with stretch-accelerated activation and deactivation. I_{mHCN2} responses to step protocols indicated that at least two transitions were mechanosensitive: an unspecified rate-limiting transition along the hyperpolarization-driven path, mode $I_{closed} \rightarrow$ mode II_{open}, and depolarization-induced deactivation (from mode I_{open} and/or from mode II_{open}). How might this affect cardiac rhythmicity? Since hysteresis patterns and "on" and "off" I_{HCN} responses all changed with stretch, predictions are difficult. For an empirical overview, we therefore clamped patches to cyclic action potential waveforms. During the diastolic potential of sinoatrial node cell and Purkinje fiber waveforms, net stretch effects were frequency dependent. Stretch-inhibited (SI) I_{mHCN2} dominated at low frequencies and stretch-augmented (SA) I_{mHCN2} was progressively more important as frequency increased. HCN channels might therefore contribute to either SI or SA cation conductances that in turn contribute to stretch arrhythmias and other mechanoelectric feedback phenomena.

INTRODUCTION

Mechanical forces affect the electrophysiology of cardiac and smooth muscle cells. Prime candidates for force transduction in mechanoelectric feedback are channels whose open probability changes reversibly with membrane stretch, i.e., mechanosensitive (MS) channels. MS channels include (along with TRP, 2PDK, and others) voltage-gated channels (1). Here, we examine stretch responses of hyperpolarization-activated cyclic nucleotide-gated (HCN) channels, the only cation-selective voltage-gated channels (2). HCN tetramers form pacemaker channels and the subunits have a Kv-like arrangement (six transmembrane-spanning domains each with S1–S4 sensor modules and S5–S6 pore modules).

Highlighting the need to test pacemaker channel mechanosensitivity are the following observations: 1), cell swelling reversibly increases I_{mHCN2} (3); 2), swelling of ventricular myocytes, cells now known to express HCN channels (e.g., (4,5)), activates an unidentified inwardly rectifying I_{cation} (6); 3), hypothalamic osmosensory neurons have a swelling- and voltage-dependent Cs-blockable I_{cation} (7); 4), cholesterol is a bilayer mechanical reagent that modulates voltage-gated channels (8) and altered cholesterol levels in sinoatrial node (SAN) cells alter the kinetics of HCN4-based pacemaker channels (9); 5), inhibitors of another type of MS cation conductance that is a candidate mechanotransducer for mechanoelectric feedback, the MS TRP channels, inhibit neither mouse SAN cell MS I_{cation} (10) nor certain ventricular mechanoelectric feedback phenomena (11); 6), repeated attempts to record MS TRP-like events from adult cardiomyocytes have failed (12); and 7), many MS cells and MS cellular structures are abundantly endowed with HCN channels (Table 1).

Information on native cell MS voltage-gated channel responses is sparse, but in smooth muscle and SAN cells, voltage-gated calcium channel current reversibly increases with stretch (1) (in recombinant calcium channels this trait resides with the pore subunit (13)). MS modulation of voltage-gated channels is best understood for Kv channels, where voltage sensing, slow inactivation, and a concerted step before pore opening have all been characterized as MS transitions (14,15). Reversible stretch responses in these Kv channels occur in both excised and cell-attached patches (16); and since patch excision destroys membrane skeleton organization, we infer that the bilayer transmits force. Why does Kv gating respond to bilayer stretch? We hypothesize that each conformation of a Kv channel's extensive protein/bilayer interface (17) has a sufficiently different lateral pressure profile (18) that bilayer mechanical perturbations change the relative stabilities of the conformations. Lateral pressure profiles can be perturbed physically (i.e., bilayer expansion/

Submitted July 19, 2006, and accepted for publication November 7, 2006.

Address reprint requests to Catherine E. Morris, Neuroscience, Ottawa Health Research Institute, Ottawa Hospital, Ottawa, Ontario, Canada K1Y 4E9. Tel.: 613-798-5555 ext. 18608; Fax: 613-761-5330; E-mail: cmorris@ohri.ca.

0006-3495/07/03/1559/14 $2.00

doi: 10.1529/biophysj.106.092478

TABLE 1 HCN-based channels in mechanosensory/ motile structures

Osmosensory neurons—hypothalamic osmosensory magnocellular neurons of the supraoptic nucleus have a pharmacologically identified I_h (pacemaker current) (49); although osmosensitivity requires expression of a truncated vanilloid receptor (43), the identity of the SI osmosensitive background cation conductance is unresolved
Baroreceptor terminals (50)—HCN1, 2, and 4 isoforms are expressed in mechanoreceptor endings of aortic arch mechanosensory neurons
Sperm flagella (21)—immunocytochemistry (sea urchin isoforms) locates spHCN expression in the sperm flagellum and not in the head. Human testis is HCN4-rich, but cellular, and the subcellular localization in that tissue is unknown (51)
Vertebrate saccular hair cells (52)—in situ hybridization (subcellular localization unknown)
Primary afferents/pain (re: tactile allodynia, ectopic discharge) (53)—pharmacological inhibition of pacemaker current relieves tactile allodynia. Centrally, HCN2 widely colocalizes with substance P (54).
Urinary bladder afferents (L6-S1 spinal chord, dorsal root ganglion neurons) (HCN2 is the predominant type of HCN channel expressed; possible involvement in the micturation reflex) (55)
Primary sensory afferents/enteric nervous system (56) I_h currents and positive immunoreactivity for HCN1, 2, and 4 but not for HCN3
Dorsal root ganglion sensory afferents Cell bodies have I_h, are immunopositive for HCN1 and HCN2 (57)

compression) and/or chemically (e.g., depletion/enrichment of surface-active lipids, alcohols, anesthetics, and drugs). Since the ''bilayer mechanics'' of membrane stretch and the bilayer mechanics of cholesterol, lysophospholipids, short chain alcohols, phenothiazines, etc. are related forms of lipid stress (19), the fact that HCN channels can be modulated by stretch has wide potential physiological and pathophysiological implications.

Our principal subject here, mHCN2, is known to participate in SAN cell and neuronal rhythmicity through the phenotypes of a knockout mouse (20). We also briefly tested spHCN (21) (from sea urchin) since this is the only isoform for which gating current information has been obtained (22) and the one for which it was shown that HCN and Kv1 voltage sensors respond similarly to voltage (23). In HCN channels, however, it is hyperpolarization, not depolarization, that triggers channel opening. In Kv1 channels, depolarization and stretch facilitate the same step, namely, the independent depolarization-driven activation transition (15). On the face of it, if HCN channels respond like Kv1 channels, then stretch should slow I_{HCN} activation and speed I_{HCN} deactivation. However, that is not the full story. Kv1 channel mutants with identified rate-limiting transitions reveal additional MS transitions: stretch accelerates slow inactivation (15) and it decelerates a concerted voltage-dependent step just before pore opening (14). If comparable transitions occur in HCN channels (not yet established in the case of concerted transitions), they may be similarly MS.

Mode switching, a kinetic trait whose consequences become striking during prolonged voltage excursions, is a feature common to HCN and Kv channels (22). The Kv1 version is termed ''C-type inactivation''. Depending on recent voltage history, Kv1 channels are in ''active'' or ''slow-inactivated'' mode; ''active'' has open and closed states, ''slow-inactivated'', only closed states. In HCN channels, by contrast, both modes have open and closed states and hence discrete g (V) curves (Fig. 1 *A*). Mannikko et al. hypothesize (22) that once a HCN channel opens, a voltage-independent conformation change occurs at the pore/sensor domain interface that stabilizes the voltage sensor in its retracted position and thus gives rise to a depolarizing shift in the Q (V) and activation curves. Mammalian HCN1, 2, and 4 isoforms all exhibit mode-switch behavior which, for all of them, occurs on a 100-ms timescale even though activation kinetics vary by well over an order of magnitude (HCN1 is fastest, HCN4 is slowest) (24). The resulting hysteresis in the HCN channel current/voltage (I/V) relations is most prominent in HCN1 and least in HCN4 (25). Prolonged depolarization favors (stabilizes) mode I and prolonged hyperpolarization favors mode II (Fig. 1 *A*) with the overall consequence that open HCN channels experience longer openings and closed ones, longer closings.

Cardiomyocytes express mixtures of isoforms HCN1, 2, and 4 (26). Smooth muscle shows electrophysiological and reverse transcription-polymerase chain reaction evidence of HCN2, 3, and 4 (27). In mammalian brain, all four isoforms are expressed, each with a unique pattern of distribution (28); immunogold electronmicroscopy shows that, as well as being expressed in neurons, HCN2 has a widespread expression in oligodendrocytes (29). Native HCN-based channels, with conductances of <10 pS, pass Ca^{2+} (30) as well as Na^+ and K^+.

We expressed HCN channels in oocytes, monitoring macroscopic I_{HCN} in cell-attached patches before, during, and after stretch, using a variety of voltage clamp protocols. In Kv1 channels depolarization elicits activation of closed channels, and the process accelerates with stretch (15). In HCN channels, depolarization elicits deactivation of open channels, and we predicted it too would accelerate with stretch since it involves comparable motions of the voltage sensors (23). Thinking of HCN channels as ''inverted Kv1 channels'' we therefore expected to observe ''stretch inhibition'' (SI) during hyperpolarization (due to stretch-enhanced deactivation). We were therefore surprised to observe a very unequivocal ''stretch augmentation'' (SA). Eventually we found that, indeed, deactivation was accelerated with stretch, but this strong effect was initially cryptic, since a), it did not result in a slower activation of I_{HCN} during hyperpolarizations, and b), we did not immediately understand the workings of HCN channels protracted tail currents.

Having unexpectedly found that HCN current activation accelerated with stretch, a second surprise came when we tested currents during rhythmic activity. During slow action potential (AP) waveforms, the SI effects, not the SA effects, were what dominated. More particularly, during the diastolic part of APs, I_{mHCN2} showed SI at low and SA at high ''beat''

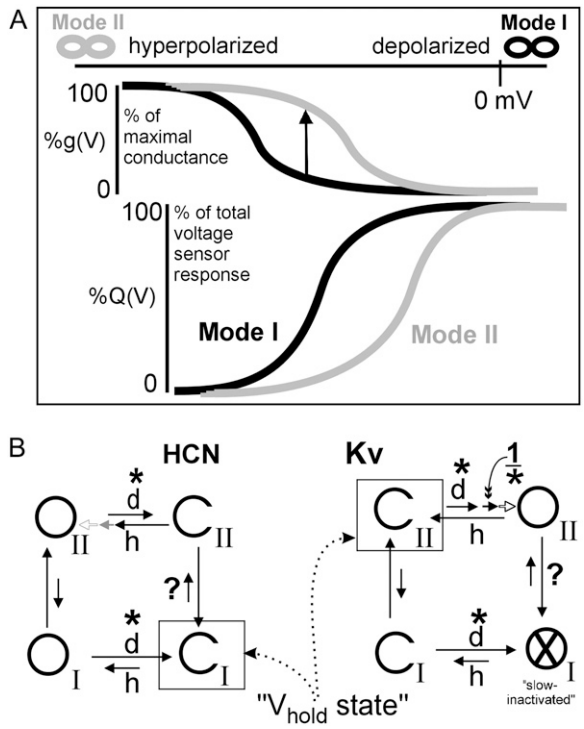

FIGURE 1 Modes and a common kinetic framework for HCN and Kv channels. (*A*) After prolonged sojourns (∞) at hyperpolarized or depolarized voltages, HCN channels principally occupy mode II (*gray*) or mode I (*black*) (22), respectively. Activation and gating charge curves (g (V), Q (V)) for the modes are depicted. The vertical arrow depicts the consequence (at a given voltage) of undergoing a mode I to mode II transition. (*B*) Open (O) and closed (C) states connected in circular schemes (22) for HCN and Kv channels (d, depolarization; h, hyperpolarization). The x through the O_I of Kv signifies that in Kv-WT, ''O_I'', unlike its HCN counterpart, is occluded (i.e., ''inactivated-nonconducting'') (see Discussion). The dominant states for typical V_{hold} potentials (depolarized-HCN; hyperpolarized-Kv) are boxed. Asterisks and inverse asterisks signify candidate stretch-accelerated and stretch-decelerated transitions, respectively, that would represent a consistent pattern across subfamilies. Two additional candidates for stretch-accelerated transitions bear question marks (see Discussion). The stretch-decelerated (1/*) Kv transition (14) is the concerted depolarization-driven closed-closed transition just before the last (voltage-independent) pore opening step (67,68). Whether HCN channels have analogous concerted transitions (shown *gray*) into the open state(s) is unknown. The asterisks in mode II correspond to a known stretch-accelerated voltage sensor motion for Kv (15); evidence suggesting that the comparable mode I transition is also stretch-accelerated is presented here for mHCN2.

frequencies. It required the emerging understanding of HCN channel mode switch and the hysteresis that results from mode switch (22) to help clarify the time-dependent stretch responses of the mHCN2 pacemaker channels.

METHODS

Oocyte preparation and cRNA injection

Xenopus laevis oocytes were injected with 5–55 ng cRNA as described previously (14). Capped cRNA for mHCN2 (mHCN2-pGEM-HE (kindly provided by Steve Siegelbaum); linearized with SphI) (31) and spHCN (21) (SPIH-pGEM-HE (kindly provided by U. B. Kaupp (21)); linearized with NheI) was produced by in vitro transcription using Ambion message machine.

Electrophysiology

Manually devitellinated oocytes were transferred to an inverted microscope rig. Thick-walled, sylgard-coated, fire-polished (using a soda glass-coated platinum filament) pipettes were prepared as previously (14) and had resistances of 2–4 MΩ. Macroscopic currents measured from cell-attached patches (Axopatch 200B; Axon Instruments, Foster City, CA) at RT (20°C–22°C) were filtered at 5 kHz (Axopatch 200B low-pass filter) and analyzed using WinASCD (Guy Droogmans) and Origin (Microcal, Northampton, MA).

Experimental voltage protocols (step, ramp, and waveform protocols) were controlled via pClamp 8, as indicated in Results. V_{hold} was 0 mV unless otherwise noted.

Membranes were stretched reversibly via negative pipette pressure, controlled, and monitored by a DPM-1B transducer (Bio-Tek Instruments, Winooski, VT) or a high-speed pressure clamp (HSPC-1, ALA Scientific Instruments, Westbury, NY). MS responses were typically elicited using −30 or −40 mmHg. Because a given pressure generates a different tension in different patches, several levels were sometimes tested. To obtain difference currents, protocols were structured as Before/During/After stretch (*B*/*D*/*A*) sets, with at least 15 s between runs within a *B*/*D*/*A* set. Data were discarded when stretch-induced changes were irreversible.

Water-injected (in actuality, Tris buffer-injected) control oocytes were incubated for 2–3 days, patched and clamped using protocols like those used for Figs. 2–88 (i.e., step, ramp, and AP clamp protocols) to make *B*/*D*/*A* sets (using −40 mm Hg or more). The same lanthanum (1 mM), high-K pipette solution was used for control oocytes as for HCN expressing oocytes. The control records (available online as Supplementary Material) showed virtually no evidence of time- and voltage-dependent conductances.

Solutions

High-K solution (for bath and pipette) contained (in mM) 89 KCl, 0.4 $CaCl_2$, 5 HEPES, 0.8 $MgCl_2$ (pH 7.5 with KOH). Then 40 μM $GdCl_3$ or 1 mM $LaCl_3$ was added to pipettes to block the endogenous MS cation channels. Lanthanum (adopted partway through the project) was always fully effective. Gadolinium was sometimes fully effective, but sometimes MS cation channel activity made records unusable, despite adding degassed acidified stock solution (100 mM $GdCl_3$) to degassed pipette solution immediately before recording (32). Either gadolinium precipitated imperceptibly or oocytes sporadically express La-sensitive-Gd-insensitive $I_{MScation}$ channels; renal cells (33) reportedly have such channels.

RESULTS

Monitoring recombinant HCN channels against an $I_{MScation}$ background

To illustrate why lanthanides were needed, Fig. 2 *Ai* shows a ''worst-case'' example of interference by endogenous $I_{MScation}$. A hyperpolarizing ramp was applied before, during, and after stretch (*B*/*D*/*A*). Here and throughout, black/red/gray signify *B*/*D*/*A*. The *B* and *A* traces run along the *x* axis, and $I_{MScation}$ (i.e., the current elicited by stretch, the *D* trace) corresponds to ~40 open MS_{cation} channels. In Fig. 2 *Aii*, as in 2 *Ai*, −100-mmHg suction was used, but there was no stretch current because 40 μM gadolinium in the pipette inhibited $I_{MScation}$. I_{HCN} families in the presence of lanthanides are shown in Fig. 2 *Bi* and *ii* (mHCN2; 40 μM

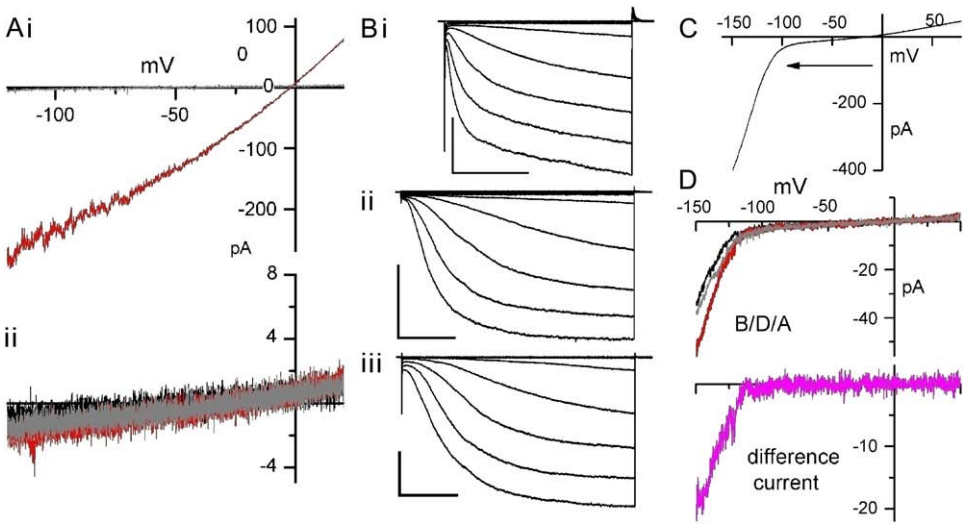

FIGURE 2 Dealing with the endogenous MS cation channel. (*A*) Ramp (33 mV/s) currents on patches from uninjected oocytes before, during, and after (*B/D/A*: *black*, *red*, *gray*) stretch without (*i*) or with (*ii*) 40 μM Gd^{3+} in the pipette. Typically, stretch was applied using less intense suction than the −100 mmHg used here. (*B*) spHCN1 (*i*) and I_{mHCN2} (*ii* and *iii*) current families, using 20-mV steps from a V_{hold} of 0 mV (*i*) or +20 mV (*ii*, *iii*) to −140 mV (*i* and *iii*) or −160 mV (*ii*), with 40 μM Gd^{3+} (*i*, *ii*) or 1 mm La^{3+} (*iii*) in the pipette; scales 200 pA/0.5 s; 100 pA/0.25 s; and 200 pA/0.2 s (*i–iii*). (*C*) A typical inwardly rectifying ramp I_{HCN} (33 mV/s) for mHCN2; arrow indicates ramp direction. (*D*) Ramp currents (as in *C*) with a *B/D/A* protocol, using strong suction (−80 mmHg); in the $I_{diff} = D - [(B + A)/2]$, the small instantaneous component gets removed.

gadolinium and 1 mM lanthanum chloride, respectively) and 2 *Biii* (spHCN; 40 μM gadolinium chloride). A hyperpolarizing ramp (Fig. 2 *C*) reveals the minor ohmic component reversing at ~0 mV (comprising the instantaneous component (34) $I_{HCNinst}$, nonspecific I_{leak}, and any imperfectly inhibited $I_{MScation}$) and $I_{HCN\ (V,t)}$ for mHCN2 channels, most of which would have been in mode I as they activated at ~−100 mV. The *B/D/A* ramp traces in Fig. 2 *D* show that inhibiting $I_{MScation}$ (as in Fig. 2 *Bii*) allowed for extraction of a stretch difference current, I_{diff} (i.e., $D - [(B + A)/2]$), shown in pink.

Capacitive transients interfered with early I_{HCN} during voltage steps (e.g., Figs. 3 *A* and 4 *A*). Nevertheless, we used no online linear subtraction since that requires long excursions to mode-switch-inducing voltages and would obliterate any stretch changes in $I_{HCNinst}$. Traces are either raw current, averaged replicates (2 or 3), or I_{diff} (i.e., $D - [(B + A)/2]$ from a *B/D/A* protocol). ''Stretch-augmented'' (SA) and ''stretch-inhibited'' (SI) correspond to ''inward'' and ''outward'' I_{diff}, respectively.

A priori, stretch might alter unitary HCN channel conductance. Since smooth muscle (35) cells show large (>50 pS) hyperpolarization- and stretch-activated I_{cation} events, sporadic unitary events riding atop macroscopic I_{mHCN2} during stretch (e.g., Fig. 3 *B*) were of interest. However, brief depolarizations showed that such events never inwardly rectified, and since they never occurred with La^{3+} (see Methods), we take them to be endogenous currents.

Stretch increases I_{HCN} during hyperpolarizing steps

Fig. 3 *A* shows that hyperpolarization-induced I_{mHCN2} was accelerated and augmented by stretch. As is common for recombinant I_{HCN}, sporadic inward noise (e.g., as in *red* and *gray traces*) was sometimes seen at large hyperpolarizations but was unrelated to stretch. At $V_{hold} = -40$mV there was no I_{HCN} (note $I = 0$ pA at the start of traces). After prolonged hyperpolarizations, however, stepping back to −40 mV produced a sustained tail current. In other words, the 80-mV drop produced, as expected, an ohmic decrease in I_{HCN}, but this was not followed by decay toward $I = 0$. Channels stayed open. We return later to this manifestation that mode switching had occurred during the hyperpolarized sojourn.

As seen in Fig. 3 *B*, even with Gd^{3+} in the pipette, patches sometimes exhibited inward and outward unitary $I_{MScation}$ events. The events contaminating two of the stretch traces illustrate a stark difference between MS I_{HCN} and endogenous $I_{MScation}$: even at the few pA level, MS I_{HCN} was ''macroscopic''. Moreover, endogenous unitary $I_{MScation}$ was not time dependent (note the unitary events during the latent period for the voltage- and time-dependent component of I_{mHCN2}) (see also Fig. 5 *A* (*x*, *bottom*)).

Stretch does not affect the instantaneous component of I_{mHCN2}

Not only did stretch not induce inwardly rectifying high conductance states of the mHCN2 channels, it did not alter $I_{mHCN2inst}$. This was directly evident from the insensitivity to stretch of $I_{mHCN2inst}$ in records where the voltage- and time-dependent component of I_{mHCN2} increased with stretch. This lack of effect is apparent by inspection of the latent periods for I_{mHCN2} in Fig. 3 *B* (see also Fig. 5 *C* and Fig. 6, *A* and *B*) and by inspection of hyperpolarizing ramps without and with stretch in Fig. 2 *D* (see also Fig. 7, *B* and *C*).

Activation of spHCN is stretch sensitive

In *B/D/A* sets, I_{spHCN} (Fig. 4 *A*) exhibited stretch-accelerated activation (*arrows*). As a semiquantitative measure of the

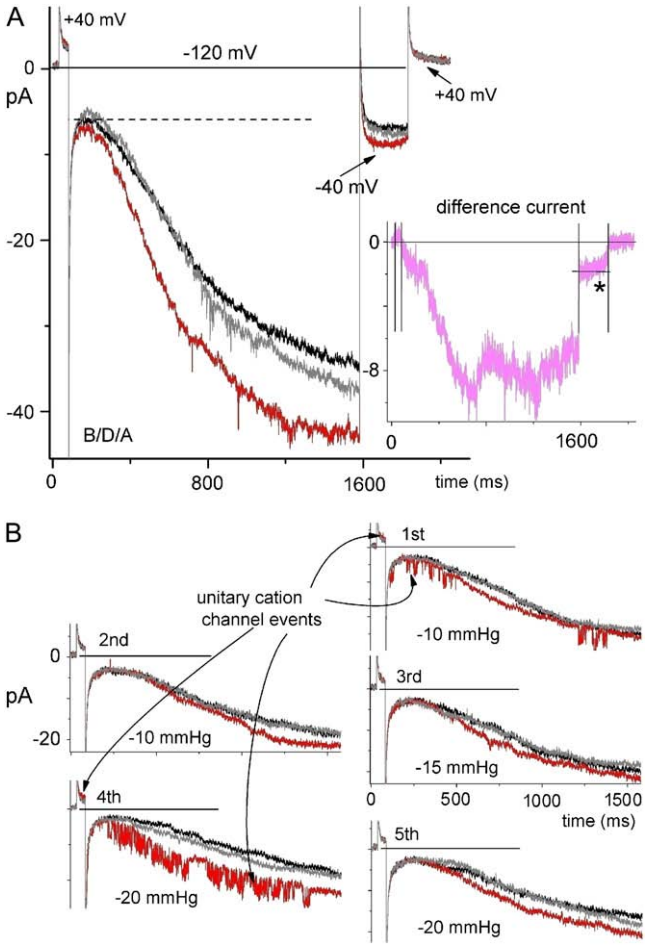

FIGURE 3 Stretch, oocyte patches, mHCN2, and the subcomponents of I_{mHCN2} 40 μM Gd^{3+} present. $V_{hold} = -40$ mV. (*A*) Averaged I_{mHCN2} for two sequential *B/D/A* sets (*D*, −30 mmHg). Notable are the large instantaneous current component (evident at −120 mV above the *dashed line*) and the effect of stepping back to V_{hold}. I_{diff} for the averaged sets is plotted at right. The asterisk is mentioned in the text. (*B*) Five sequential B/D/A sets (*D*, as indicated in mmHg). The voltage protocol was to +40 mV then to −120 mV as in *A*. The unitary currents are discussed in the text.

effect of stretch (using −30 mmHg) note that, for more than 150 ms, more than half of the time- and voltage-dependent component of I_{spHCN} comprised SA I_{HCN} (Fig. 4 *B*). I_{diff} peaked at ~150 ms for all three stretch intensities tested (Fig. 4 *C*). Qualitatively, the traces show unequivocal reversible acceleration of activation by stretch, but as the expanded I_{diff} sections show, the early difference currents were too nonuniform to allow for standardized curve fitting and assignment of rates (as was true, too, for mHCN2 activation currents).

Stretch-augmented and stretch-inhibited I_{mHCN2}: current activation and tail currents

Fig. 5 *A* shows I_{mHCN2} for an unusually stable patch: first a control set, then three *B/D/A* sets (with $D = -20$ mmHg; these are averaged in Fig. 5 *B*). (We did not attempt to study tail currents at positive depolarized voltages; the brief steps to +40 mV were internal controls to ensure that endogenous MS channels were inhibited.) Stretch-accelerated activation resulted in an elevated steady-state I_{mHCN2}. On stepping to −40 mV, the magnitude of tail I_{diff} (*pink arrow*) reflects the stretch augmentation of current that had occurred at −110 mV. The persistence of I_{diff} at −40 mV (which, note was also V_{hold}) suggests that mode switch had occurred during the sojourn at −110 mV (at hyperpolarized voltages, the channels prefer mode II with its right-shifted g (V)). Stretch evidently reversibly affected a rate-limiting transition along the pathway mode $I_{closed} \rightarrow$ mode II_{open} (i.e., the path that is suggested by the vertical arrow in Fig. 1 *A*). Longer tail currents than obtained here were needed to clarify the shape and polarities of I_{diff} (Fig. 5 *B**).

At −40 mV, tail currents required ~2 s for completion, as seen in Fig. 6 *A*. At right, the I_{diff} for the $D = -50$ mmHg *B/D/A* set is shown below that for the $D = -30$ mmHg set (acquired before the −50 mmHg set). Tail currents exhibited an open-channel latency (~100 ms) after which stretch reversibly accelerated the decay of I_{HCN} to zero. Note that tail I_{diff} (*pink*) was initially stretch augmented, but then crossed the zero current line and became stretch inhibited (likewise, Fig. 6 *C**). The inflection (after ~0.5 s) in the Fig. 6 *A* tail I_{diff} simply indicates the approach to steady state (likewise for spHCN, Fig. 4, for inflections in the rising phase I_{diff} and for the rising phase I_{diff} here at −140 mV).

Stretch acceleration of I_{mHCN2} deactivation was robust. In the four *B/D/A* sets of Fig. 6, *B–D*, the hyperpolarizing prepulse was successively deepened (−80, −100, −120, −140 mV). At the onset of the −40 mV tail currents, the post −140 mV case (Fig. 6 *D*, *bottom*) should have the greatest fraction of channels in mode II_{open}. Whether or not the latent period, which is clearly evident as the flat portion in the Fig. 6 *C* tail I_{diff}, was stretch sensitive is uncertain. The shorter latency here at −50 mm Hg than at −30 mmHg in Fig. 6 *A* (see the I_{diff} traces) suggests that it might be. The latency presumably included ''electrically silent'' mode $II_{open} \rightarrow$ mode I_{open} transitions and (as per the expanded version of the Mannikko et al. model (22)) independent S4 motions between the (multiple) open states of either mode. The deactivation phase, which would include mode $I_{open} \rightarrow$ mode I_{closed} and mode $II_{open} \rightarrow$ mode II_{closed} transitions, was, however, unequivocally accelerated by stretch. This is the response depicted by the asterisk in Fig. 1 *B**, HCN.

Thus, stretch accelerated I_{mHCN2} activation during hyperpolarization and I_{mHCN2} deactivation during depolarization. In mHCN2, therefore, at least two types of transition (with opposing effects on current) were susceptible to the bilayer mechanical perturbation (36) produced by membrane stretch.

Our data showed that the ''sign'' (SA versus SI) of I_{diff} at a given voltage (and time) depended on voltage history. We emphasize this because it would be crucial in designing *B/D/A* stretch tests for any native $I_{pacemaker}$ and in interpreting the outcomes. Consider Fig. 6 *D*, where a 0.7-s depolarization to −40 mV had four different ''histories''. During that 0.7 s,

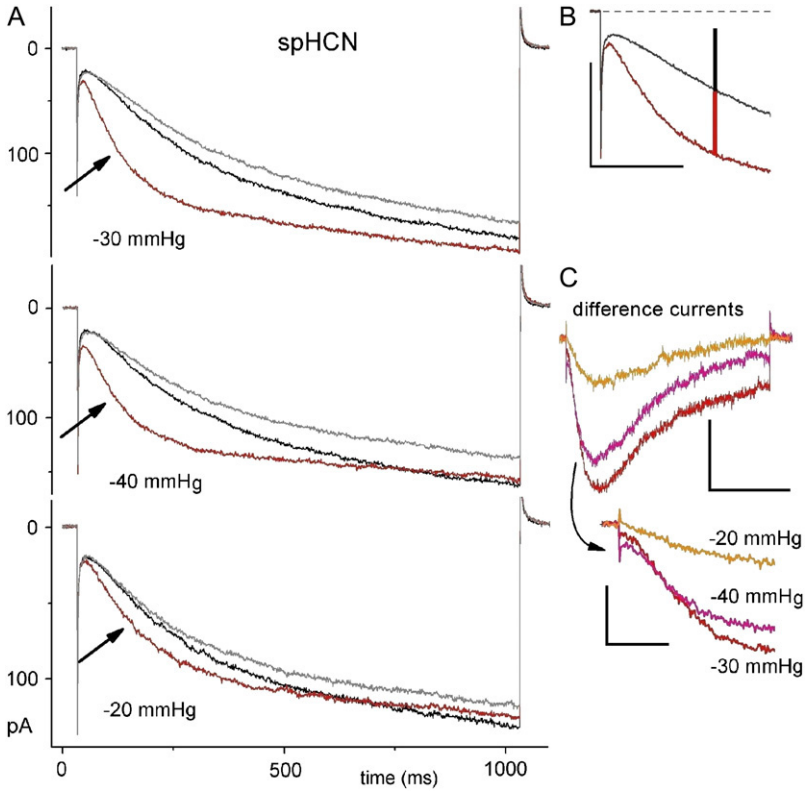

FIGURE 4 spHCN1 and stretch. (*A*). Three *B*/*D*/*A* sets recorded (same patch) in the sequence shown. The protocol was a simple step from 0 mV to −80 mV. The consistently smaller amplitude of the after traces (*gray*) within each *B*/*D*/*A* and the progressive decrease in the amplitudes of before traces (*black*) from one *B*/*D*/*A* indicates that slow rundown was occurring, but this did not prevent stretch acceleration of activation. (*B*) Expanded early part of the first *B*/*D*/*A* set (i.e., $D = -30$ mmHg; *black trace* is ($B + A$)/2) with vertical red and black bars of equal amplitude. (*C*) I_{diff} for these *B*/*D*/*A* sets, with early section expanded. Scale bars (*top* to *bottom*); 100 pA/150 ms/, 30 pA/400 ms, 30 pA/60 ms.

I_{diff} was mostly SA post −80 mV but mostly SI post −140 mV. With mode switching plus stretch acceleration (on both the activation and deactivation pathways) taken into account, this makes sense. Where there is net SA during hyperpolarization, the I_{diff} must start out SA, but given time they all become SI current (post −80 mV, 0.7 s was clearly not sufficient time). Except for being prematurely truncated, the Fig. 6 *D* tail currents behave as in Fig. 6 *A* (likewise for Fig. 3 *A** and Fig. 5*). Consider, in Fig. 6 *A*, the small SI I_{diff} at −80 mV versus, in Fig. 6 *B*, the (eventual) SA I_{diff} at −80 mV. This too is perfectly understandable in terms of mode switch plus dual stretch effects but would be perfectly confusing if voltage history was ignored. Specifically, after a sojourn (>1 s) at −40 mV, mode I_{closed} would dominate, but (as the SI traces for I_{diff} at −30 mmHg and −50 mmHg Fig. 6 *A* reveal) stretch-accelerated deactivation caused further closure. Consequently, during stretch, a step to −80 mV produced what was initially an SI I_{diff}. Given sufficient time at −80 mV, as seen in Fig. 6 *B*, activation (presumably into mode II_{open} far more than into mode I_{open}) began and stretch-accelerated activation began to overwhelm the effect of stretch on deactivation, thus producing the net SA effect.

Voltage hysteresis: dual effects of stretch during sawtooth ramps

HCN voltage hysteresis (25) during sawtooth ramp clamp is typified by right-shifted, more S-shaped I/V relations in depolarizing limbs (22). For HCN channels, unlike Kv channels, moderate slowing of ramp speeds fails to make hyperpolarizing and depolarizing limbs converge (22). Though hysteresis is less pronounced in mHCN2 than in mHCN1 (24,25), mHCN2 (with 1 mM La in the pipette) nevertheless showed the characteristic pattern noted for mHCN1 (i.e., increased rather than decreased hysteresis as ramps are made moderately slower (22)), as seen in Fig. 7 *A*. The hysteresis persisted during stretch (Fig. 7 *B*). For the first (hyperpolarizing) limb, applying stretch was essentially like running a slower ramp; I_{mHCN2} increased. For the (second) depolarizing limb, stretch and ramp speed (= voltage history) interacted strongly (Fig. 7 *Ci* and *ii*). At first glance, only SA current is apparent, but that reflects the voltage history of the ramp protocol: the sawtooth ramps, like typical HCN step protocols, started from depolarized voltages. Fig. 7 *Ciii* shows a normalized plot of stretch and no-stretch traces for the slower (i.e., closer to equilibrium) sawtooth pair. This plot demonstrates, in relative terms, clear evidence of stretch-accelerated deactivation of I_{mHCN2} (i.e., clear evidence of ''SI behavior'') in the depolarizing limb. In some patches (not shown) the effect of stretch on deactivation was sufficient to yield outward difference current in the depolarizing limb. Thus, step and sawtooth protocols yielded a consistent pattern of SA plus SI effects.

Dual effects of stretch during AP waveforms

Rhythmic cardiac AP represent even more complex voltage histories than sawtooth ramps. Lacking appropriate kinetic

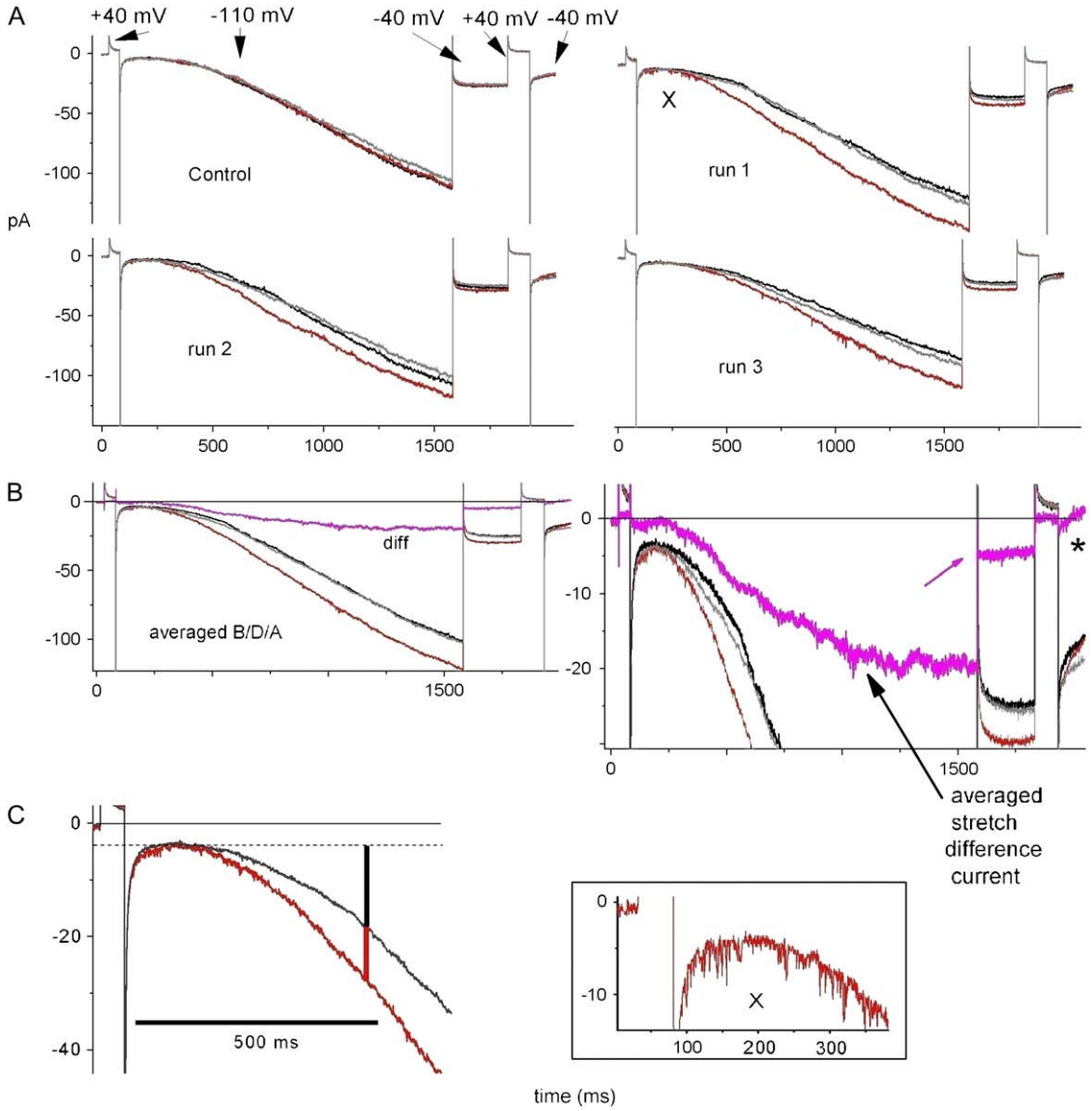

FIGURE 5 Reversible, reproducible stretch changes in I_{mHCN2}. (*A*) Four sequential *B*/*D*/*A* sets. $V_{hold} = -40$ mV, followed by the indicated steps. Gadolinium was used. The boxed trace (*bottom*) expands ''run 1, *D*'' near the X, to show unitary endogenous events. For control run, $D = 0$ mmHg, for runs 1–3, $D = -20$ mmHg. (*B*) Averaged traces and I_{diff} (expanded at *right*). Asterisk, nearly overlooked stretch-accelerated current decline. (*C*) For runs 1–3, expanded stretch (averaged *D*) and no-stretch (averaged $(B + A)/2$) segments from above show that $I_{mHCN2inst}$ was stretch insensitive and that for ~500 ms, >1/3 of the time-dependent I_{mHCN2} was due to stretch.

data for cardiac modeling, we looked empirically at MS I_{mHCN2} during APs. I_{mHCN2} before, during, and after stretch was compared from patches clamped to cyclic AP waveforms. This was complicated by the fact that the amplitude of I_{mHCN2} changed systematically with AP frequency (it was smaller at lower frequencies) and by the fact that during low frequency runs, stretch often decreased I_{mHCN2} irreversibly. Nevertheless, when a given patch was successfully tested (i.e., when reversible stretch-induced changes were obtained) at more than one frequency, the outcome for SAN cell-like AP excursions was as is seen in Fig. 8 *A*: during a train of APs a small amount of SA occurred at high frequency (e.g., 533 bpm (beats per minute)), whereas a larger SI occurred at low frequency (e.g., 15 bpm). Fig. 8, *B–D*, and *F* shows data for a single patch at three frequencies: 60 bpm showed SI and 240 bpm and 480 bpm showed SA. Fig. 8 *C* shows higher resolution excerpts, and Fig. 8 *D* shows their I_{diff} (overlying the voltage waveform). Fig. 8 *E* (different patch) shows three 60 bpm trials with the AP hyperpolarizing to three different extents. Reversible SI occurred in each case, with the effect accumulating over several APs then, poststretch, decaying over several APs.

The I/V relations (*B*/*D*/*A*; $B + A$ averaged) for APs (e.g., Fig. 8 *F*) revealed that with the membrane potential driven by AP waveforms, mHCN2 channels furnished the membrane with a cation conductance whose degree of inward

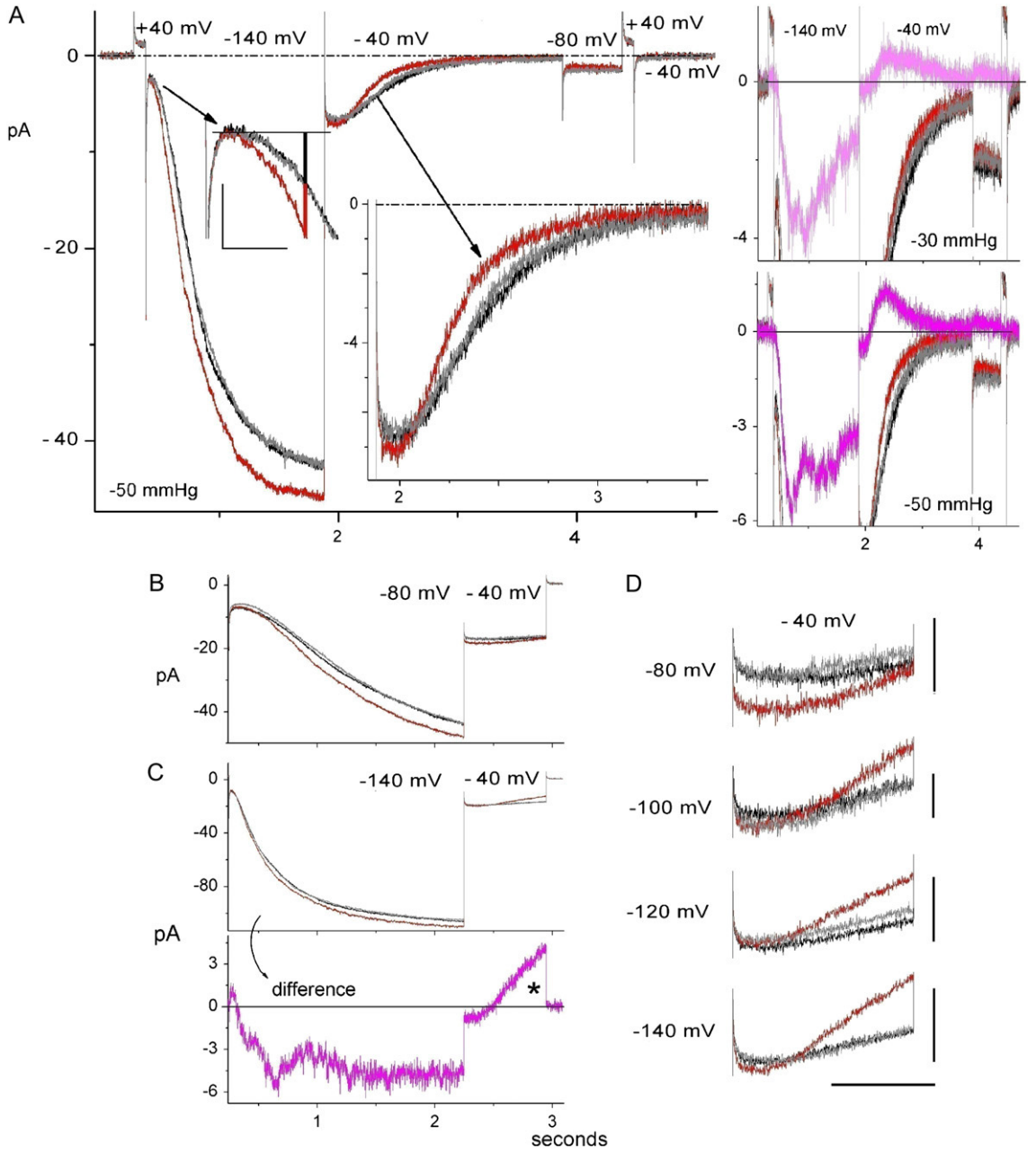

FIGURE 6 Effect of stretch on I_{mHCN2} activation and deactivation. (*A*) *B*/*D*/*A* with early activation (scales, 4 pA, 0.1 s; *red-black bar* as in Fig. 4 *A*) and deactivation expanded; for ~150 ms after the hyperpolarizing step, ~1/2 the time-dependent I_{mHCN2} was SA. The −50 mm Hg I_{diff} is shown, bottom right (with its *B*/*D*/*A* for reference) and above, the equivalent for a smaller stretch stimulus. The prolonged (2 s) step to −40 mV showed that after a latency, stretch accelerated the current decline. The I_{diff} shapes here clarify those from truncated protocols (Figs. 3 and 5). (*B* and *C*) *B*/*D*/*A* traces, as explained in the text, plus an I_{diff} for which an asterisk ($I_{cation} > 0$ pA) indicates SI I_{mHCN2}. (*D*) expanded I_{tail} at −40 mV for this series of *B*/*D*/*A* sets (labels identify the preceding hyperpolarization level). Vertical scales from top to bottom: 3 pA, 2 pA 5 pA, 5 pA; horizontal scale: 0.4 s. $V_{hold} = -40$ mV. Lanthanum was used here and in subsequent figures.

rectification was far weaker than expected from g (V) relations implied by voltage step families or by hyperpolarizing ramp clamp (such as in Fig. 2, *B* and *C*). Well-behaved pacemaker current is generally seen as being ''on'' during the diastolic potential of an AP and ''off'' during most of the spike (37); indeed, HCN1 behaves in this way (25). However, the outcome we noted—namely that, with or without stretch, AP waveforms keep mHCN2 channels disequilibrated at relatively high open probability throughout the AP regime—accords with recent observations of Azene et al. (25; see their Fig. 4 *B*) for HCN2 and HCN4.

The SAN waveforms were nearly sinusoidal, so we checked for SI/SA effects in a more asymmetrical waveform. Fig. 8 *G* shows I_{mHCN2} for a patch driven to a Purkinje fiber

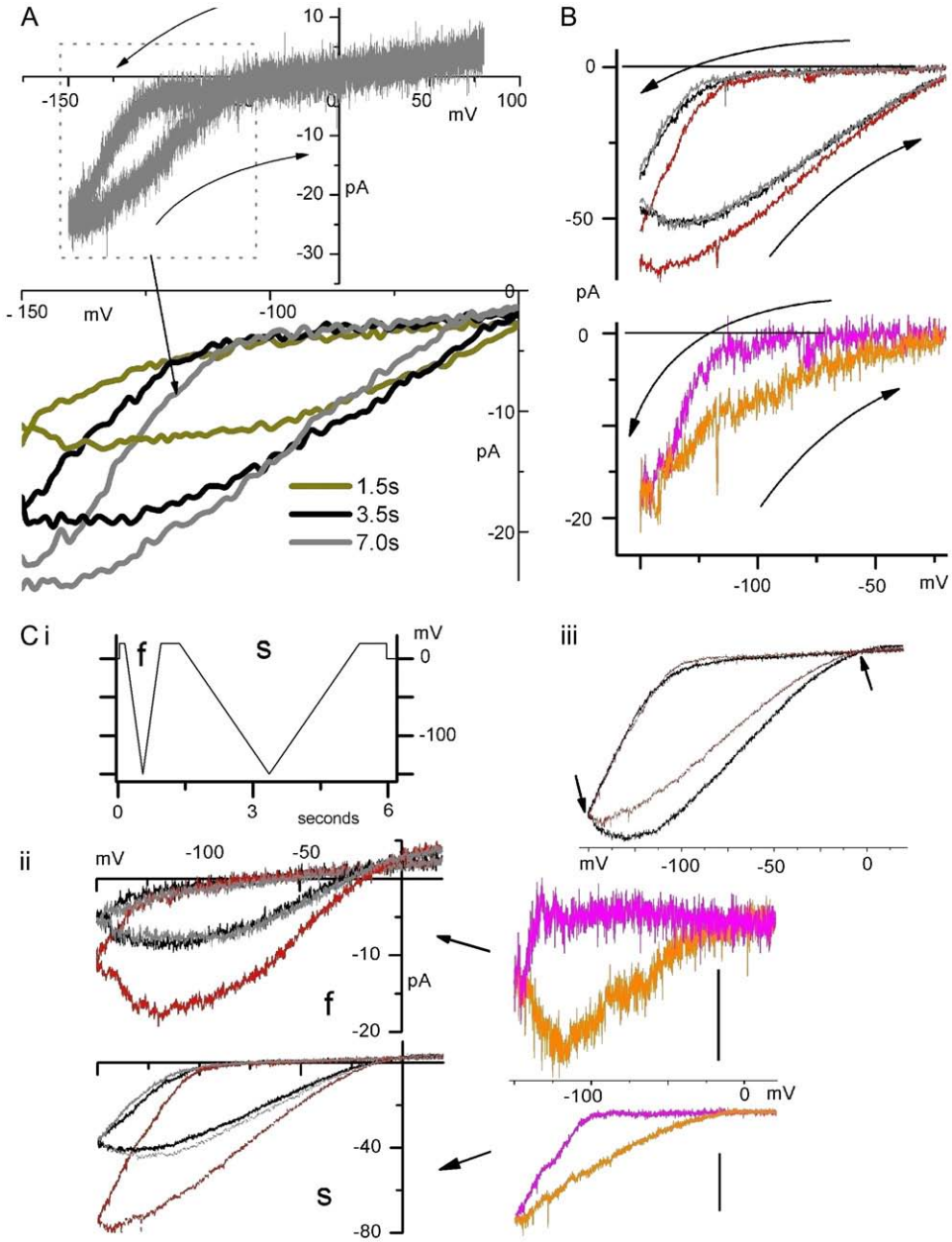

FIGURE 7 Hysteresis and sawtooth ramp I_{mHCN2} (*A*) Top, a hyperpolarizing then depolarizing ramp set (with a 50-ms pause at −150 mV) from +80 mV to −150 mV. A heavily filtered segment from this ramp set and from two others at higher speeds (same patch) is shown below (labels give the duration of each limb). (*B*) A *B*/*D*/*A* ramp set (*D*, −40 mmHg, ramps as in *A*, 7.0 s) and its I_{diff}. (*C*) *i*. The fast-then-slow ramp protocol for the *B*/*D*/*A* set ($D = -40$ mmHg) seen in *ii* with fast (f) and slow (s) sets plotted separately alongside their respective I_{diff}, for which scales are 4 pA (fast) and 10 pA (slow). In *iii*, relative effects of stretch on rates in the two limbs are compared graphically for the slow *B*/*D*/*A* by normalizing (see *arrows*) the average no-stretch ((*B* + *A*)/2) and the stretch (*D*) I/V relations.

type AP (−90 to +5 mV) at 120 then at 480 bpm (*inset*). In both cases the net effect of stretch was SI behavior; at 240 bpm (not shown) stretch produced an intermediate effect in terms of the extent and rate of SI. For this waveform, reversible stretch effects were obtained for six patches tested at two or more frequencies (30–480 bpm). SI always dominated at the lower frequencies, but the frequency at which the SI/SA balance tipped had a wide range. One patch, e.g., showed SI at 60 bpm and a mixed response at 120 bpm (initial SA subsiding to SI over the nine-beat stimulus).

These findings serve as a ''proof of principle'' demonstration that during rhythmic activity, a given population of HCN channels can mediate both an SI and an SA cation conductance. The kinetic particulars of homotetrameric channels operating with elevated extracellular K^+ at room temperature in an oocyte bilayer without auxiliary subunits are not, of course, those of native channels. For native channels in situ, therefore, the SI/SA balance might play out very differently. In diverse situations native pacemaker channels may feel bilayer stretch during voltage excursions. These include the following: the SAN during excessive filling of the right atrium, hypothalamic osmosensory neurons during lowered blood osmolarity, smooth muscle cells in distended gut, blood vessels, and bladder. What our data indicate is that under these conditions, the SI/SA balance of the pacemaker channels can be expected to vary with the waveform of the cell in question and with the duration of the stretch stimulus.

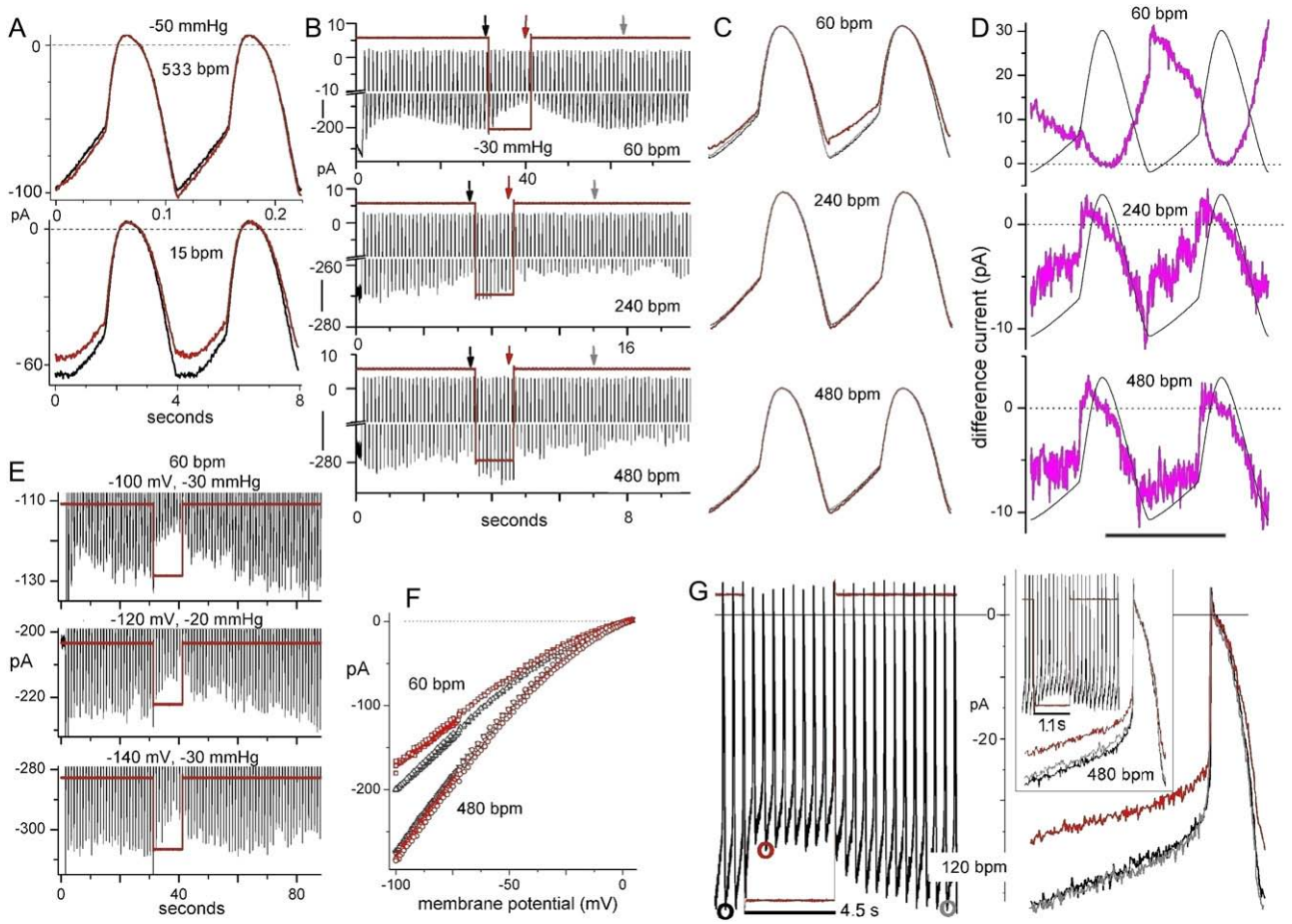

FIGURE 8 Rhythmic AP currents before during and after stretch. The data in *A*, *E*,and *G*, and *B*, *C*, *D*, and *F* are from four different patches clamped to a rhythmic SAN cell-like AP waveform (*A–F*) or to a Purkinje fiber-like AP waveform (*G*). All the figures except *F* (which has I/V relations for AP currents before and during stretch at the indicated beat frequencies) and *D* (in which stretch difference currents overlie the voltage waveform) are raw current traces. In *B*, the vertical arrows locate the traces shown in *C*. Vertical scales (in *B*) included for the bottom segment of each of the three current traces are 20, 10, and 10 pA for 60, 240, and 480 bpm, respectively. In *A* and *C*, before and after traces overlap. Other details are given in the text.

DISCUSSION

The MS responses of HCN channels

Using recombinant homotetrameric HCN channels expressed in oocytes at levels that yielded macroscopic current, we measured patch current before, during, and after membrane stretch, with pipette suction used to apply stretch. We observed no effect of stretch on the amplitude of the instantaneous component of mHCN2 current. Overall, it appeared that, as in Kv channels (15), stretch altered HCN channel gating kinetics without inducing any novel states. In Kv1 channels, the independent depolarization-driven motions of the voltage sensor accelerate with stretch (15), so for HCN channels we thought that stretch-accelerated HCN deactivation might impede hyperpolarization-induced activation of I_{HCN}. But for neither of two distantly related HCN channels was that true. In both a sea urchin and a mouse isoform, stretch accelerated the activation of I_{HCN}. Further characterization was done with the mouse isoform, mHCN2. During voltage steps, both I_{mHCN2} activation (hyperpolarization-induced) and deactivation (depolarization-induced) accelerated reversibly with stretch. Sawtooth ramp clamp (hyperpolarize-then-depolarize) revealed a voltage hysteresis that persisted with stretch.

To predict stretch responses of I_{mHCN2} during APs or to model them from our qualitative information about MS responses was not feasible. Instead, we clamped patches to rhythmic AP waveforms then applied stretch. Like others (25), we found that rhythmic AP waveforms kept HCN channels disequilibrated at a high open probability; operational I/V relations (I_{mHCN2} versus V_m during rhythmic AP clamp, e.g., +5 mV to −100 mV at 1 Hz) reflected open channel permeation at least as much as voltage-dependent gating. These I/V curves contrast starkly with those from hyperpolarizing ramp clamp (i.e., passing through 0 mV and heading to −150 mV), which elicited no current before

~ -100 mV. During APs, given patches exhibited net SI and net SA responses, depending on waveform; but overall, at lower frequencies, it was SI that dominated.

SI dominance in APs might seem surprising given the strong showing of SA effects with step and sawtooth ramp clamp. However, in those protocols, typical depolarized V_{hold} levels created a bias for the MS responses of hyperpolarization-induced transitions, which, it turned out, were SA effects. Cardiac excitability machinery (mimicked here by AP clamp) keeps V_m more hyperpolarized, so our quasiphysiological waveforms had the opposite bias from that of our steps and ramps. During slow AP depolarizations (diastole), deactivation of mHCN2 channels comes increasingly into play. If, as we suspect, stretch accelerates deactivation transitions of HCN (both modes), domination by SI during slow APs seems reasonable—likewise for slow sawtooths, where SI was apparent but only after depolarization was underway. Substantial delays precede deactivation of mHCN2, perhaps explaining why SI effects accumulated over the course of several APs (and decayed in the same fashion upon stimulus release). With higher frequency APs, the interplay of dV/dt and channel kinetics evidently made mHCN2 channels hover closer to their open states. The characteristic abruptness of the net SA effects seen at high frequencies (fast onset and offset with stretch) was striking. The next section discusses which channel motions might be candidates for MS transitions.

Possible MS transitions

Generically speaking, for a two-state channel, stretch-accelerated activation of current could arise from reduced stability of the closed state (accelerated opening transition) and stretch-accelerated deactivation could arise from reduced stability of an open state (accelerating closing transition). If stretch stabilized the transition state (like a catalyst, lowering the barrier between the two states), both rates would accelerate. Practically speaking, in I_{mHCN2}, neither activation nor deactivation is a kinetically simple (e.g., first order) process, so we could not attribute MS responses to specific transitions. As a proxy, since HCN and Kv channels have similar voltage-induced gating motions, we consider identified MS transitions of Shaker Kv channels (Fig. 1 *B*). With both protein structure and gating motions being largely conserved, the forces that structure the protein-bilayer interface are likely to be broadly conserved. The unified model of Kv and HCN mode switch (22) provides an elegant framework for comparing MS responses of HCN and Kv channels.

In Fig. 1 *B*, in keeping with that framework, major HCN and Kv transitions are shown in circular four-state kinetic schemes. The two modes are labeled; mode I corresponds, in Kv, to the slow inactivated mode. The Mannikko et al. scheme (22) highlights 4 states (drawn from a 20-state model), but here, concerted transitions (two *short arrows* in mode II) are also suggested. They are depicted in mode II only, since it is for mode II in Kv that such transitions have been identified (14). For typical voltage clamp experiments, V_{hold} would be ~ -100 mV and ~ 0 mV for Kv and HCN, respectively, keeping channels closed in mode II and mode I, respectively, as indicated. The existence of a Kv mutant with an ''inactivated''-conducting state (38) (''inactivated'' in that prolonged depolarization left shifts its Q (V) curve) helps validate and explain the common Kv/HCN framework.

Vertical arrows signify mode-switch transitions and horizontal ones (except the *short open arrow*), charge-displacing voltage sensor motions. Based on the left-shifted Q (V), Mannikko et al. (22) suggest HCN mode-switch motions are molecularly related to Kv slow inactivation motions. Kv activation and Kv slow inactivation accelerate to the same extent with stretch, as if the two processes have near identical S4/bilayer interactions and thus experience the same bilayer mechanical perturbation during stretch (15). Based on simultaneous gating (and/or ionic) currents and residue-specific optical measurements as well as more extensive optical scans (39–41), Kv slow inactivation (including the earliest P-inactivation step) is thought to involve lateral S4 motions, that is, a net motion in the plane of the bilayer. This makes the sensitivity of Kv slow inactivation to bilayer stretch (15) eminently reasonable. The voltage-independent stretch-sensitive motion presumably includes the initial (P type) slow-inactivation process (i.e., the mode $II_{open} \rightarrow$ mode $I_{inactivated}$ switch). A question mark on the relevant mode switch transition in Fig. 1 *B* suggests that stretch acceleration here might explain stretch-accelerated slow inactivation in Kv channels. That picture would be even more appealing, however, if it could explain our HCN channel observations in a straightforward way, but it cannot. To explain the stretch-accelerated activation seen in HCN channels, stretch would have to accelerate opposite-going transitions, as indicated by the question mark at $C_I \rightarrow C_{II}$ for HCN. Given the proclivity of HCN channels for ''inverted gating'', however, this is a possibility.

For HCN, stretch acceleration of a rate-limiting forward transition in the path mode$I_{closed} \rightarrow$ modeII_{open} (*up arrow*, Fig. 1 *A*) would accelerate I_{HCN} activation as would stretch deceleration of a fast back-reaction. These possibilities are not mutually exclusive. As explained in the Fig. 1 *B* legend, asterisks indicate the class of voltage-dependent transitions identified in Kv as stretch-and-depolarization accelerated (15). HCN tail current data showed that, after a latency, stretch speeded up the depolarization-induced deactivation of I_{mHCN2}. The simplest explanation for this, namely that deactivation of HCN channels (both modes) is a stretch and depolarization accelerated process, would be consistent with the Kv activation picture. The inverse asterisk in Fig. 1 *B* marks a voltage-dependent transition that, in Kv, decelerates with stretch (14); this last depolarization-driven motion before pore opening is a concerted step. In a Kv mutant whose concerted opening steps happen to be rate limiting (Shaker ILT), this stretch-decelerated transition yields SI

activation (14), but it is not known if HCN channels open via comparable (albeit hyperpolarization-driven and thermal) concerted motions (depicted in *gray* in Fig. 1 *B*).

Physiological and pharmacological implications of MS transitions in HCN channels

Cardiac mechanoelectric feedback phenomena are thought to require an $I_{MScation}$ (10,12,42). TRP-based channels are prime candidates in neurons, as they are in osmosensory neurons (43), another rhythmically active cell, but based on our observations, it will also be important to ask if the HCN-based cation channels in these cells transduce physiologically relevant force signals. During stretch and swelling, guinea pig (low intrinsic beat rate) and mouse (high intrinsic beat rate) SAN preparations make opposite responses, the former showing increased and the latter decreased rhythmicity (10). Our core finding is that HCN channels can generate both SA and SI cation current. Thus native pacemaker channels are now candidate contributors to these and similar responses. Since the SI/SA balance in our experiments produced net SI behavior at slower beat rates and net SA behavior at faster ones, it will be important to test a variety of native HCN channels in different mammalian models subjected to swelling and stretching stimuli before speculating further. The recombinant channels, of course, lacked auxiliary proteins that are likely present in situ and may tune the channels differently (44). Commenting on work by Zicha et al. (45), Giles (46) points out that during atrial flutter, the slow rate of native HCN channel deactivation manifests as what could be considered a steady-state current (e.g., as in Fig. 8 *F*). If, in such circumstances, the slowness of deactivation is rate limiting, stretch-accelerated deactivation might have an appreciable impact.

In addition to osmosensory neurons (which exhibit an osmosensory SI cation conductance; see references in Liu et al. (7) and Naeini et al. (43)) HCN channels are abundant in (see Table 1) baroreceptor nerve terminals, various primary afferent mechanosensory neurons, hair cells, and sperm (where, we note, spHCN expression is restricted to the high-curvature, mechanically dynamic flagellar membrane). In these locations, the mechanosensitivity of HCN channels might provide a tunable element for mechanotransduction and/or electromotility.

With two distantly related HCN channels now included among the MS voltage-gated channels, mechanosensitivity can be regarded as a family-wide trait for voltage-gated channels. The gating of all voltage-gated channels types (8,19), including HCN channels (Table 2), is susceptible to many bilayer mechanical (18) reagents. It is likely that the susceptibilities of voltage-gated channels to bilayer stretch and to such reagents are both responses to lipid stress perturbations, one being physical, the other, physicochemical. Classic models of S4-sensor motions kept the sensor sequestered in the channel protein, away from lipids, but now, some S4 residues are known to contact bilayer lipids (17,47). The stretch and voltage dependencies of specific Kv channel transitions (14,15) constitute proof that physically induced lateral pressure profile changes alter gating rates. We suggest that the MS kinetics of mHCN2 and Kv channels follow a common pattern (Fig. 1 *B*) because broad conservation of structure in voltage-gated channels dictates robust conservation of bilayer mechanics. If so, modulation of voltage-gated channels by broad-spectrum lipophilic reagents may involve the same voltage sensor and gate transitions that are perturbed by membrane stretch. If this holds, much pharmacological perplexity evaporates (14,19,48). There would be no need to invoke halothane, ethanol, propofol, cholesterol, and capsazepine ''binding sites'' in HCN channels to explain kinetic modulation by these bilayer mechanical reagents (see Table 2) any more than we need to invoke ''stretch-activation and stretch-inhibition gating motifs'' in HCN channels to explain their repertoire of stretch responses.

TABLE 2 Bilayer mechanical reagents and HCN channels

Propofol ($GABA_R$ antagonist)
1. (5 μM) I_h and I_{mHCN2}: activation slowed, conductance decreased (58)
2. (5 μM) I_h and I_{mHCN1}: activation left-shifted, conductance decreased (though not for I_{mHCN2}) (59)
Halothane, Isoflurane, Sevoflurane (60)
Inhibition, closed state stabilization (I_h and $I_{HCN1,2}$ activation left-shifted)
Capsazepine (61) (TRPV antagonist)
(8 μM) Inhibits I_{hHCN1} (activation left-shifted, slowed)
Clonidine (62) (α-adrenergic antagonist)
Putative direct inhibition of $I_{pacemaker}$
Cholesterol depletion (9)
I_{HCN4} activation right-shifted, deactivation slowed. Similar findings in SAN cells.
Ethanol (63)
I_h reversibly increased, activation accelerated
Sphingosine 1-phosphate (64)
(1 μM) decreased the α-adrenergic-induced enhancement of I (f)
Lysophosphatidylcholine (65) (a product of ischemia)
(20 μM) I (f) amplitude decreased; activation curve left-shifted.

Most of the listed studies provide evidence that the chemicals act directly (presumably via lipid stress effects) on the HCN channels, not via other proteins such as neurotransmitter receptors.
E.g., see Bahri et al. (66) for the effects of propofol on bilayer mechanical parameters.

SUPPLEMENTARY MATERIAL

An online supplement to this article can be found by visiting BJ Online at http://www.biophysj.org.

This work was supported by a grant from the Canadian Institutes of Health Research.

REFERENCES

1. Morris, C., and U. Laitko. 2005. The mechanosensitivity of voltage-gated channels may contribute to cardiac mechano-electric feedback. W. B. Saunders, Philadelphia.

2. DiFrancesco, D. 2006. Serious workings of the funny current. *Prog. Biophys. Mol. Biol.* 90:13–25.
3. Calloe, K., P. Elmedyb, S. P. Olesen, N. K. Jorgensen, and M. Grunnet. 2005. Hypoosmotic cell swelling as a novel mechanism for modulation of cloned HCN2 channels. *Biophys. J.* 89:2159–2169.
4. Arinsburg, S. S., I. S. Cohen, and H. G. Yu. 2006. Constitutively active Src tyrosine kinase changes gating of HCN4 channels through direct binding to the channel proteins. *J. Cardiovasc. Pharmacol.* 47:578–586.
5. Qu, J., C. Altomare, A. Bucchi, D. DiFrancesco, and R. B. Robinson. 2002. Functional comparison of HCN isoforms expressed in ventricular and HEK 293 cells. *Pflugers Arch.* 444:597–601.
6. Suchyna, T. M., J. H. Johnson, K. Hamer, J. F. Leykam, D. A. Gage, H. F. Clemo, C. M. Baumgarten, and F. Sachs. 2000. Identification of a peptide toxin from Grammostola spatulata spider venom that blocks cation-selective stretch-activated channels. *J. Gen. Physiol.* 115:583–598.
7. Liu, X. H., W. Zhang, and T. E. Fisher. 2005. A novel osmosensitive voltage gated cation current in rat supraoptic neurones. *J. Physiol.* 568:61–68.
8. Lundbaek, J. A., P. Birn, S. E. Tape, G. E. Toombes, R. Sogaard, R. E. Koeppe 2nd, S. M. Gruner, A. J. Hansen, and O. S. Andersen. 2005. Capsaicin regulates voltage-dependent sodium channels by altering lipid bilayer elasticity. *Mol. Pharmacol.* 68:680–689.
9. Barbuti, A., B. Gravante, M. Riolfo, R. Milanesi, B. Terragni, and D. DiFrancesco. 2004. Localization of pacemaker channels in lipid rafts regulates channel kinetics. *Circ. Res.* 94:1325–1331.
10. Cooper, P. J., and P. Kohl. 2005. Species- and preparation-dependence of stretch effects on sino-atrial node pacemaking. *Ann. N. Y. Acad. Sci.* 1047:324–335.
11. Sung, D., R. W. Mills, J. Schettler, S. M. Narayan, J. H. Omens, and A. D. McCulloch. 2003. Ventricular filling slows epicardial conduction and increases action potential duration in an optical mapping study of the isolated rabbit heart. *J. Cardiovasc. Electrophysiol.* 14:739–749.
12. Sachs, F. 2005. Stretch-activated channels in the heart. *In* Cardiac Mechano-Electric Feedback and Arrhythmias: From Pipette to Patient. W. B. Saunders, Philadelphia.
13. Calabrese, B., I. V. Tabarean, P. Juranka, and C. E. Morris. 2002. Mechanosensitivity of N-type calcium channel currents. *Biophys. J.* 83:2560–2574.
14. Laitko, U., P. F. Juranka, and C. E. Morris. 2006. Membrane stretch slows the concerted step prior to opening in a Kv channel. *J. Gen. Physiol.* 127:687–701.
15. Laitko, U., and C. E. Morris. 2004. Membrane tension accelerates rate-limiting voltage-dependent activation and slow inactivation steps in a Shaker channel. *J. Gen. Physiol.* 123:135–154.
16. Gu, C. X., P. F. Juranka, and C. E. Morris. 2001. Stretch-activation and stretch-inactivation of Shaker-IR, a voltage-gated K+ channel. *Biophys. J.* 80:2678–2693.
17. Long, S. B., E. B. Campbell, and R. Mackinnon. 2005. Voltage sensor of Kv1.2: structural basis of electromechanical coupling. *Science.* 309: 903–908.
18. Cantor, R. S. 2002. Size distribution of barrel-stave aggregates of membrane peptides: influence of the bilayer lateral pressure profile. *Biophys. J.* 82:2520–2525.
19. Morris, C. E., and P. F. Juranka. 2007. Lipid stress at play: mechanosensitivity of voltage-gated channels. *Current Topics in Membranes.* 59:297–338.
20. Ludwig, A., T. Budde, J. Stieber, S. Moosmang, C. Wahl, K. Holthoff, A. Langebartels, C. Wotjak, T. Munsch, X. Zong, S. Feil, R. Feil, M. Lancel, K. R. Chien, A. Konnerth, H. C. Pape, M. Biel, and F. Hofmann. 2003. Absence epilepsy and sinus dysrhythmia in mice lacking the pacemaker channel HCN2. *EMBO J.* 22:216–224.
21. Gauss, R., R. Seifert, and U. B. Kaupp. 1998. Molecular identification of a hyperpolarization-activated channel in sea urchin sperm. *Nature.* 393:583–587.
22. Mannikko, R., S. Pandey, H. P. Larsson, and F. Elinder. 2005. Hysteresis in the voltage dependence of HCN channels: conversion between two modes affects pacemaker properties. *J. Gen. Physiol.* 125:305–326.
23. Mannikko, R., F. Elinder, and H. P. Larsson. 2002. Voltage-sensing mechanism is conserved among ion channels gated by opposite voltages. *Nature.* 419:837–841.
24. Elinder, F., R. Mannikko, S. Pandey, and H. P. Larsson. 2006. Mode shifts in the voltage gating of the mouse and human HCN2 and HCN4 channels. *J. Physiol.* 575:417–431
25. Azene, E. M., T. Xue, E. Marban, G. F. Tomaselli, and R. A. Li. 2005. Non-equilibrium behavior of HCN channels: insights into the role of HCN channels in native and engineered pacemakers. *Cardiovasc. Res.* 67:263–273.
26. Baruscotti, M., A. Bucchi, and D. Difrancesco. 2005. Physiology and pharmacology of the cardiac pacemaker (''funny'') current. *Pharmacol. Ther.* 107:59–79.
27. Greenwood, I. A., and S. A. Prestwich. 2002. Characteristics of hyperpolarization-activated cation currents in portal vein smooth muscle cells. *Am. J. Physiol. Cell Physiol.* 282:C744–C753.
28. Monteggia, L. M., A. J. Eisch, M. D. Tang, L. K. Kaczmarek, and E. J. Nestler. 2000. Cloning and localization of the hyperpolarization-activated cyclic nucleotide-gated channel family in rat brain. *Brain Res. Mol. Brain Res.* 81:129–139.
29. Notomi, T., and R. Shigemoto. 2004. Immunohistochemical localization of Ih channel subunits, HCN1-4, in the rat brain. *J. Comp. Neurol.* 471:241–276.
30. Yu, X., K. L. Duan, C. F. Shang, H. G. Yu, and Z. Zhou. 2004. Calcium influx through hyperpolarization-activated cation channels (I (h) channels) contributes to activity-evoked neuronal secretion. *Proc. Natl. Acad. Sci. USA.* 101:1051–1056.
31. Chen, S., J. Wang, and S. A. Siegelbaum. 2001. Properties of hyperpolarization-activated pacemaker current defined by coassembly of HCN1 and HCN2 subunits and basal modulation by cyclic nucleotide. *J. Gen. Physiol.* 117:491–504.
32. Morris, C. E., P. F. Juranka, W. Lin, T. J. Morris, and U. Laitko. 2006. Studying the mechanosensitivity of voltage-gated channels using oocyte patches. *Methods Mol. Biol.* 322:315–329.
33. Hurwitz, C. G., V. Y. Hu, and A. S. Segal. 2002. A mechanogated nonselective cation channel in proximal tubule that is ATP sensitive. *Am. J. Physiol. Renal Physiol.* 283:F93–F104.
34. Proenza, C., and G. Yellen. 2006. Distinct populations of HCN pacemaker channels produce voltage-dependent and voltage-independent currents. *J. Gen. Physiol.* 127:183–190.
35. Hisada, T., R. W. Ordway, M. T. Kirber, J. J. Singer, and J. V. Walsh Jr. 1991. Hyperpolarization-activated cationic channels in smooth muscle cells are stretch sensitive. *Pflugers Arch.* 417:493–499.
36. Wiggins, P., and R. Phillips. 2005. Membrane-protein interactions in mechanosensitive channels. *Biophys. J.* 88:880–902.
37. Cohen, I. S., and R. B. Robinson. 2006. Pacemaker current and automatic rhythms: toward a molecular understanding. *Handb. Exp. Pharmacol.* 171:41–71.
38. Olcese, R., D. Sigg, R. Latorre, F. Bezanilla, and E. Stefani. 2001. A conducting state with properties of a slow inactivated state in a shaker K (+) channel mutant. *J. Gen. Physiol.* 117:149–163.
39. Loots, E., and E. Y. Isacoff. 2000. Molecular coupling of S4 to a K (+) channel's slow inactivation gate. *J. Gen. Physiol.* 116:623–636.
40. Gandhi, C. S., E. Loots, and E. Y. Isacoff. 2000. Reconstructing voltage sensor-pore interaction from a fluorescence scan of a voltage-gated K+ channel. *Neuron.* 27:585–595.
41. Pathak, M., G. Agarwal, L. Kurtz, C. S. Gandhi, and E. Isacoff. 2006. A fluorescence scan to investigate the structural dynamics of the Shaker K+ channel. Abstract No. 2268. Biophysical Society 50th Annual Meeting, 2006. http://www.biophysics.org/.
42. Zabel, M., B. S. Koller, F. Sachs, and M. R. Franz. 1996. Stretch-induced voltage changes in the isolated beating heart: importance

of the timing of stretch and implications for stretch-activated ion channels. *Cardiovasc. Res.* 32:120–130.

43. Naeini, R. S., M. F. Witty, P. Seguela, and C. W. Bourque. 2006. An N-terminal variant of Trpv1 channel is required for osmosensory transduction. *Nat. Neurosci.* 9:93–98.
44. Qu, J., Y. Kryukova, I. A. Potapova, S. V. Doronin, M. Larsen, G. Krishnamurthy, I. S. Cohen, and R. B. Robinson. 2004. MiRP1 modulates HCN2 channel expression and gating in cardiac myocytes. *J. Biol. Chem.* 279:43497–43502.
45. Zicha, S., M. Fernandez-Velasco, G. Lonardo, N. L'Heureux, and S. Nattel. 2005. Sinus node dysfunction and hyperpolarization-activated (HCN) channel subunit remodeling in a canine heart failure model. *Cardiovasc. Res.* 66:472–481.
46. Giles, W. R. 2005. Supraventricular pacemaker activity in the canine heart: contributions from HCN channels in control conditions and in a model of heart failure. *Cardiovasc. Res.* 66:430–432.
47. Cuello, L. G., D. M. Cortes, and E. Perozo. 2004. Molecular architecture of the KvAP voltage-dependent K+ channel in a lipid bilayer. *Science.* 306:491–495.
48. Arhem, P. 2004. Voltage sensing in ion channels: a 50-year-old mystery resolved? *Lancet.* 363:1221–1223.
49. Ghamari-Langroudi, M., and C. W. Bourque. 2000. Excitatory role of the hyperpolarization-activated inward current in phasic and tonic firing of rat supraoptic neurons. *J. Neurosci.* 20:4855–4863.
50. Doan, T. N., K. Stephans, A. N. Ramirez, P. A. Glazebrook, M. C. Andresen, and D. L. Kunze. 2004. Differential distribution and function of hyperpolarization-activated channels in sensory neurons and mechanosensitive fibers. *J. Neurosci.* 24:3335–3343.
51. Seifert, R., A. Scholten, R. Gauss, A. Mincheva, P. Lichter, and U. B. Kaupp. 1999. Molecular characterization of a slowly gating human hyperpolarization-activated channel predominantly expressed in thalamus, heart, and testis. *Proc. Natl. Acad. Sci. USA.* 96:9391–9396.
52. Cho, W. J., M. J. Drescher, J. S. Hatfield, D. A. Bessert, R. P. Skoff, and D. G. Drescher. 2003. Hyperpolarization-activated, cyclic AMP-gated, HCN1-like cation channel: the primary, full-length HCN isoform expressed in a saccular hair-cell layer. *Neuroscience.* 118:525–534.
53. Lee, D. H., L. Chang, L. S. Sorkin, and S. R. Chaplan. 2005. Hyperpolarization-activated, cation-nonselective, cyclic nucleotide-modulated channel blockade alleviates mechanical allodynia and suppresses ectopic discharge in spinal nerve ligated rats. *J. Pain.* 6: 417–424.
54. Papp, I., P. Szucs, K. Hollo, F. Erdelyi, G. Szabo, and M. Antal. 2006. Hyperpolarization-activated and cyclic nucleotide-gated cation channel subunit 2 ion channels modulate synaptic transmission from nociceptive primary afferents containing substance P to secondary sensory neurons in laminae I–IIo of the rodent spinal dorsal horn. *Eur. J. Neurosci.* 24:1341–1352.
55. Matsuyoshi, H., N. Masuda, M. B. Chancellor, V. L. Erickson, Y. Hirao, W. C. de Groat, A. Wanaka, and N. Yoshimura. 2006. Expression of hyperpolarization-activated cyclic nucleotide-gated cation channels in rat dorsal root ganglion neurons innervating urinary bladder. *Brain Res.* 1119:115–123.
56. Xiao, J., T. V. Nguyen, K. Ngui, P. J. Strijbos, I. S. Selmer, C. B. Neylon, and J. B. Furness. 2004. Molecular and functional analysis of hyperpolarisation-activated nucleotide-gated (HCN) channels in the enteric nervous system. *Neuroscience.* 129:603–614.
57. Tu, H., L. Deng, Q. Sun, L. Yao, J. S. Han, and Y. Wan. 2004. Hyperpolarization-activated, cyclic nucleotide-gated cation channels: roles in the differential electrophysiological properties of rat primary afferent neurons. *J. Neurosci. Res.* 76:713–722.
58. Ying, S. W., S. Y. Abbas, N. L. Harrison, and P. A. Goldstein. 2006. Propofol block of I (h) contributes to the suppression of neuronal excitability and rhythmic burst firing in thalamocortical neurons. *Eur. J. Neurosci.* 23:465–480.
59. Chen, X., S. Shu, and D. A. Bayliss. 2005. Suppression of ih contributes to propofol-induced inhibition of mouse cortical pyramidal neurons. *J. Neurophysiol.* 94:3872–3883.
60. Chen, X., J. E. Sirois, Q. Lei, E. M. Talley, C. Lynch 3rd, and D. A. Bayliss. 2005. HCN subunit-specific and cAMP-modulated effects of anesthetics on neuronal pacemaker currents. *J. Neurosci.* 25:5803–5814.
61. Gill, C. H., A. Randall, S. A. Bates, K. Hill, D. Owen, P. M. Larkman, W. Cairns, S. P. Yusaf, P. R. Murdock, P. J. Strijbos, A. J. Powell, C. D. Benham, and C. H. Davies. 2004. Characterization of the human HCN1 channel and its inhibition by capsazepine. *Br. J. Pharmacol.* 143:411–421.
62. Kroin, J. S., A. Buvanendran, D. R. Beck, J. E. Topic, D. E. Watts, and K. J. Tuman. 2004. Clonidine prolongation of lidocaine analgesia after sciatic nerve block in rats is mediated via the hyperpolarization-activated cation current, not by alpha-adrenoreceptors. *Anesthesiology.* 101:488–494.
63. Okamoto, T., M. T. Harnett, and H. Morikawa. 2006. Hyperpolarization-activated cation current (Ih) is an ethanol target in midbrain dopamine neurons of mice. *J. Neurophysiol.* 95:619–626.
64. Guo, J., K. L. MacDonell, and W. R. Giles. 1999. Effects of sphingosine 1-phosphate on pacemaker activity in rabbit sino-atrial node cells. *Pflugers Arch.* 438:642–648.
65. Hu, Y. M., Z. Zhang, R. B. Gao, and Y. Q. Xu. 1997. Effect of lysophosphatidylcholine on the pacemaker current I (f) of sheep cardial Purkinje fibers in ischemia-like condition. *Sheng Li Hsueh Pao.* 49: 513–520.
66. Bahri, M. A., B. J. Heyne, P. Hans, A. E. Seret, A. A. Mouithys-Mickalad, and M. D. Hoebeke. 2005. Quantification of lipid bilayer effective microviscosity and fluidity effect induced by propofol. *Biophys. Chem.* 114:53–61.
67. del Camino, D., M. Kanevsky, and G. Yellen. 2005. Status of the intracellular gate in the activated-not-open state of shaker K+ channels. *J. Gen. Physiol.* 126:419–428.
68. Pathak, M., L. Kurtz, F. Tombola, and E. Isacoff. 2005. The cooperative voltage sensor motion that gates a potassium channel. *J. Gen. Physiol.* 125:57–69.